Waves & Oscillations in the Solar Atmosphere:
Heating and Magneto-Seismology
Proceedings IAU Symposium No. 247, 2007
R. Erdélyi & C. A. Mendoza-Briceño, eds.

doi:10.1017/S1743921308014762

Resonant absorption in multi-stranded coronal loops

J. Terradas, I. Arregui, R. Oliver and J. L. Ballester

Departament de Física, Universitat de les Illes Balears, E-07122 Palma de Mallorca, Spain
email: jaume.terradas;inigo.arregui;ramon.oliver;joseluis.ballester@uib.es

Abstract.
We study the excitation and damping of transverse oscillations in a complex multi-stranded model of a coronal loop. By numerically solving the time-dependent magnetohydrodynamic (MHD) equations in two dimensions, we show how the global motion of the whole bundle of tubes, produced by an external disturbance, is converted into localised motions due to the process of resonant absorption. At any location in the structure two dominant frequencies are found, the frequency of the global mode (different from the kink frequency of the individual strands) and the local Alfvén frequency. The mechanism of mode conversion is not affected by the complicated geometry of the system and for certain configurations the energy conversion does not only take place at the external edge of the composite loop but also inside the structure.

Keywords. waves, (magnetohydrodynamics:) MHD, Sun: Corona, Sun: magnetic fields

1. Introduction

The resonant conversion of wave energy from global large scale motions to localised Alfvén modes has been invoked as a possible candidate to explain the damping of coronal loop oscillations (Hollweg & Yang 1988; Goossens *et al.* 1992; Ruderman & Roberts 2002; Goossens *et al.* 2002, Terradas *et al.* 2006a). The theoretical models that have been studied so far are simple but necessary to understand the main properties of this damping mechanism. The most popular models are smooth transition layers, slab models and straight cylindrical loops. Other effects have been also investigated. The effects of background flows have been investigated for example by Hollweg *et al.* (1990) and Erdélyi & Goossens (1996). The curvature effect has been studied by Van Doorsselaere *et al.* (2004) and Terradas *et al.* (2006b), and the influence of stratification along the loop has been analysed by Andries *et al.* (2005) and by Arregui *et al.* (2005). The effect of non-circularity of the tube cross-section has been analysed by Ruderman (2003) and Ruderman & Erdélyi (2004), while the effect of the internal structure in loops has been studied by Arregui *et al.* (2007). The overall conclusion of these recent investigations is that these new ingredients do not significantly change the damping per period of the oscillations. This suggests that resonant absorption is a robust mechanism whose efficiency is not easily affected by second-order effects.

Nevertheless, the new models are still too simple compared with the real conditions in coronal loops. For example, there is observational information suggesting that loops are not monolithic (as they are usually modelled) but that they are formed by bundles of individual strands considered as mini-loops for which the heating and plasma properties are approximately uniform in the transverse direction (Schmeltz *et al.* 2005). This view is supported by some authors (Martens *et al.* 2005, Klimchuck 2006) but not by others (Aschwanden & Nitghtingale 2005, Aschwanden 2005).

The purpose of this paper is to study the effect of the internal structure and arbitrary geometry on the damped transverse coronal loop oscillations. We use a composite loop

model and we adopt a direct approach, instead of calculating the eigenmodes of the structure, which is difficult due to the complicated geometry, we investigate the dynamical response of the loop to an initial disturbance. This allows us to analyse how the energy from the global mode is converted into localised motions in the inhomogeneous regions of the loop.

2. Model and Governing MHD Equations

In our model the magnetic field is straight, uniform and pointing in the $z-$direction, $\mathbf{B} = B_0\,\hat{\mathbf{e}}_\mathbf{z}$. We adopt the zero$-\beta$ approximation, under such condition the density profile can be chosen arbitrarily. To model a bundle of loops we use a superposition of tiny, parallel tubes with different radii and densities. In Cartesian coordinates, the cross-section of the density of each individual strand is assumed to have following form,

$$\rho_i(x,y) = \rho_{0i}\,\exp\left[-\frac{(x-x_i)^2+(y-y_i)^2}{a_i^2}\right], \tag{2.1}$$

where ρ_{0i} is the maximum density of the strand, x_i and y_i the position of the strand axis and a_i the strand half-width. The density of the multi-stranded model composed of N strands is simply defined as

$$\rho_0(x,y) = \sum_{i=1}^{N}\rho_i(x,y) + \rho_e, \tag{2.2}$$

ρ_e being the density of the external medium. In Fig. 1 the two-dimensional distribution of the density (the cross section of the composite loop) is plotted for a particular configuration based on Eqs. (2.1) and (2.2). We see that in this model the loop density has an inhomogeneous distribution with a quite irregular cross section. This model has a complex geometry compared with the usual cylindrical tube or even the elliptical cross section model studied by Ruderman (2003) and Ruderman & Erdélyi (2004).

To study small amplitude perturbations in this equilibrium we use the linearised ideal MHD equations. The equilibrium depends on x and y but it is independent of the vertical coordinate z. For this reason, we Fourier analyse in this direction assuming a dependence of the form $e^{-ik_z z}$. We concentrate on the fundamental mode, with $k_z = \pi/L_0$, being L_0 the length of the loop (here we use $L_0 = 20L$, L being the typical mean tube radius). Under these assumptions the MHD equations are,

$$\rho_0\frac{\partial v_x}{\partial t} + \frac{B_0}{\mu}\left(ik_z b_x + \frac{\partial b_z}{\partial x}\right) = 0\ , \tag{2.3}$$

$$\rho_0\frac{\partial v_y}{\partial t} + \frac{B_0}{\mu}\left(ik_z b_y + \frac{\partial b_z}{\partial y}\right) = 0\ , \tag{2.4}$$

$$\frac{\partial b_x}{\partial t} + B_0 ik_z v_x = 0\ , \tag{2.5}$$

$$\frac{\partial b_y}{\partial t} + B_0 ik_z v_y = 0\ , \tag{2.6}$$

$$\frac{\partial b_z}{\partial t} + B_0\left(\frac{\partial v_x}{\partial x} + \frac{\partial v_y}{\partial y}\right) = 0\ , \tag{2.7}$$

where $\mathbf{v} = (v_x, v_y, 0)$ is the velocity and $\mathbf{b} = (b_x, b_y, b_z)$ is the perturbed magnetic field.

https://doi.org/10.1017/S1743921308014762 Published online by Cambridge University Press

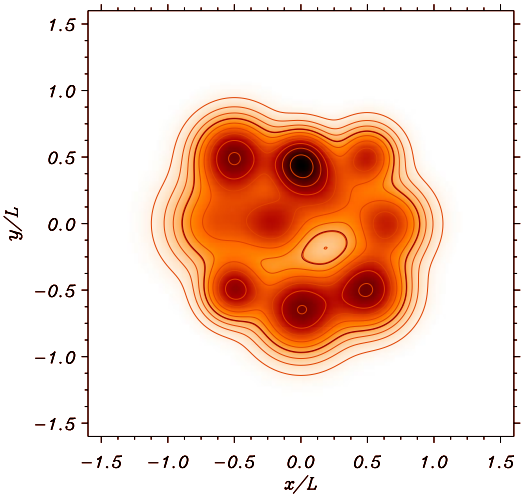

Figure 1. Cross section of the density of our multi-stranded loop model. For this particular configuration the loop is composed of 10 individual strands with widths that vary from $0.2L$ to $0.3L$. The external density is $\rho_e = 1/3\,\rho_{00}$, ρ_{00} being the maximum value of the density inside the loop. The contours represent curves of constant Alfvén frequency (given by Eq. (4.1)). The thick line corresponds to the Alfvén frequency that matches the frequency of the global mode. The lengths are normalised to L.

The initial perturbation is located in the external medium and for simplicity we assume the following form

$$v_y(x,y) = v_{y0}\ \exp\left[-\frac{(y-y_0)^2}{w^2}\right], \tag{2.8}$$

where y_0 is the position of the centre of the disturbance and w is its width (here we use $y_0 = 3L$ and $w = L$). All other MHD variables are initially set to zero. This perturbation is a planar pulse which produces the excitation of fast MHD waves that propagate and interact with the loop structure.

3. Numerical Method

To numerically solve the time-dependent MHD equations, Eqs. (2.3)−(2.7), together with the initial condition, Eq. (2.8), we use the code CLAWPACK (LeVeque 2002). This code implements a wide class of methods for solving linear or nonlinear hyperbolic problems. One of the difficulties of the problem that we are studying is the small spatial scales that are generated in the inhomogeneous layers. The resolution must be sufficiently high to resolve the different scales. For this reason we have performed high resolution simulations (typically with a grid of 4000×4000 points). To avoid significant reflections we have applied transparent boundary conditions at the domain limits, located at $x_B = \pm 8L$, $y_B = \pm 8L$. In order to better interpret and visualise the results the plots are displayed in a small spatial domain ($[-1.6L, 1.6L] \times [-1.6L, 1.6L]$).

4. Results and Discussion

The initial pulse produces a displacement of the whole ensemble of strands basically in the $y-$direction. Due to the effect of the line-tying the system periodically oscillates

https://doi.org/10.1017/S1743921308014762 Published online by Cambridge University Press

with certain frequencies. An analysis inside the loop shows that there are two dominant frequencies at each point, one is the collective frequency of the bundle of loops (different from the kink frequency of the individual strands) and the other is the local Alfvén frequency. In our configuration the Alfvén frequency is

$$\omega_A(x,y) = k_z v_A(x,y) = k_z \frac{B_0}{\sqrt{\mu\rho_0(x,y)}}, \tag{4.1}$$

and it depends on x and y. Contours of constant ω_A are represented in Fig. 1 with continuous lines.

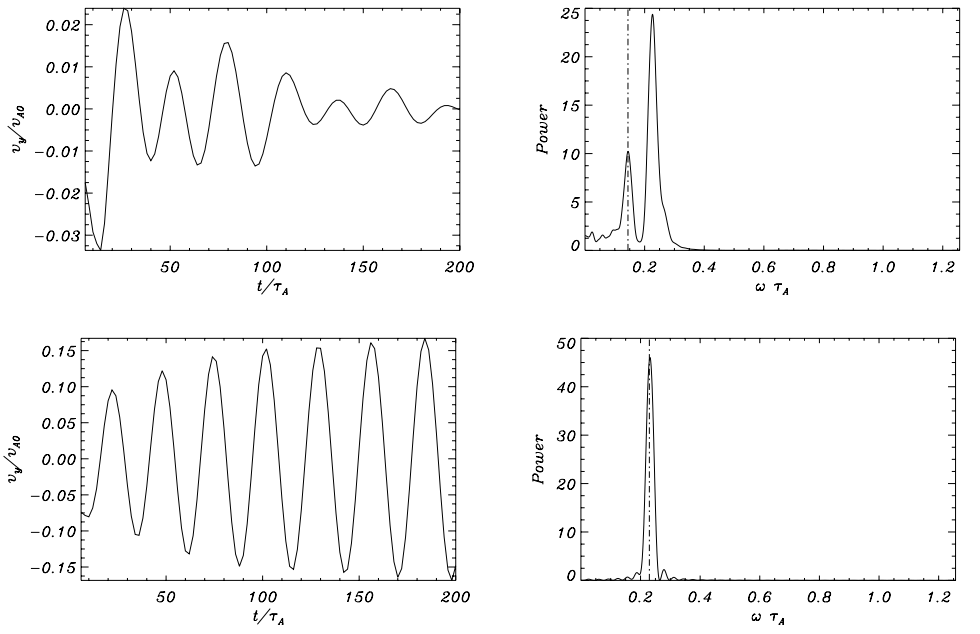

Figure 2. *Left panels:* Time evolution of the v_y velocity component at two different positions, $x = 0.0L$, $y = 0.5L$ and $x = 0.9L$, $y = 0.0L$. *Right panels:* Power spectrum of the corresponding velocity signal. The local Alfvén frequencies, calculated from the function $\omega_A(x,y)$, at the coordinates of the previous points are represented with dot-dashed lines. The time is normalised to the Alfvén transit time $\tau_A = V_{A0}/L$.

The collective frequency is the result of the excitation of the global mode of the system. In Fig. 2 (upper row) the v_y velocity component as a function of time and its power spectrum are represented at an interior point ($x = 0.0L$, $y = 0.5L$). The two dominant frequencies, the local Alfvén frequency and the global frequency (with the largest power) are clearly identified. Note also the strong decrease of the amplitude with time. On the other hand, in Fig. 2 (lower row) we see that at the point $x = 0.9L$, $y = 0.0L$ the behaviour of the signal is completely different. There is just one single peak since the local and the global frequencies coincide. At this position the amplitude of the v_y velocity component grows with time.

To explain these two different behaviours we need to understand the evolution of the whole system. In Fig. 3 the evolution of the velocity field is shown at different times in two dimensions. We can see that after the excitation large amplitude velocities develop specially near the loop boundaries. This is the consequence of the energy conversion between the global mode and the Alfvén modes. Due to this process the global oscillation

https://doi.org/10.1017/S1743921308014762 Published online by Cambridge University Press

losses its energy and its amplitude is attenuated in time (see for example the length of the arrows at the centres of the individual strands in Fig. 3 for $t = 160\,\tau_A$ or the amplitude of the oscillations in the upper left panel of Fig. 2). This eventually causes that only the local Alfvén modes remain. The excitation of these modes is already known, specially in driven problems (see for example Mann *et al.* 1995, Tirry *et al.* 1997 and Goossens & De Groof 2001). An interesting question here is the amount of energy that is deposited in these modes (this issue is addressed in Terradas *et al.* 2007). On the other hand, the amplitude of the Alfvén modes increases at the resonant layers where the energy conversion takes place (see the large arrows at the loop boundaries in Fig. 3 and see also the lower left panel of Fig. 2). Since the Alfvén frequency changes with position these modes get out of phase very quickly due to phase mixing (see also Terradas *et al.* 2006a in a cylindrical loop). The consequence of this process is visible at the external boundaries where strong shear motions develop (see the large arrows, aligned with the contours of the Alfvén frequency, oscillating in opposite directions).

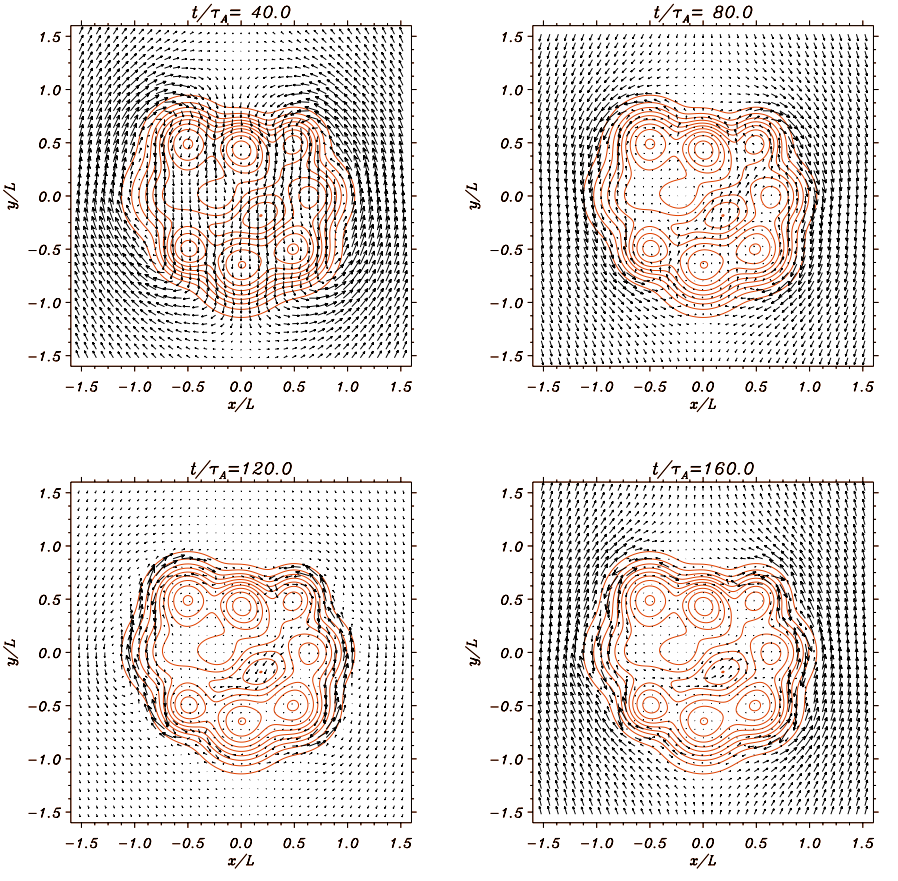

Figure 3. Time evolution of the velocity field. The loop initially oscillates in the y direction with the global mode. Due to the mode conversion motions localised on the magnetic surfaces develop (see the contours of constant Alfvén frequency represented with continuous lines). The velocity in the interior points attenuates due to the transfer of energy to the resonant layers.

To illustrate the process of energy conversion it is useful to calculate the wave energy as a function of time. In our system there are only contributions from the kinetic and

https://doi.org/10.1017/S1743921308014762 Published online by Cambridge University Press

the magnetic energy,

$$E = \frac{1}{2}\left[\rho_0\left(v_x^2 + v_y^2\right) + \frac{1}{\mu}\left(b_x^2 + b_y^2 + b_z^2\right)\right]. \tag{4.2}$$

This quantity is represented in Fig. 4 at different times (same as in Fig. 3). The plots show that the system evolves from a situation where the energy is more or less uniformly distributed to a state where it is very concentrated around the resonant layers (see the dark areas on the left and right loop edge). In fact the system evolves so that at $t = 160\,\tau_A$ the resonance energy width is quite small (see Mann *et al.* 1995 and Terradas *et al.* 2006a). Note also that the energy decreases with time at the interior points, except for the area around $x = 0.25L$, $y = -0.25L$.

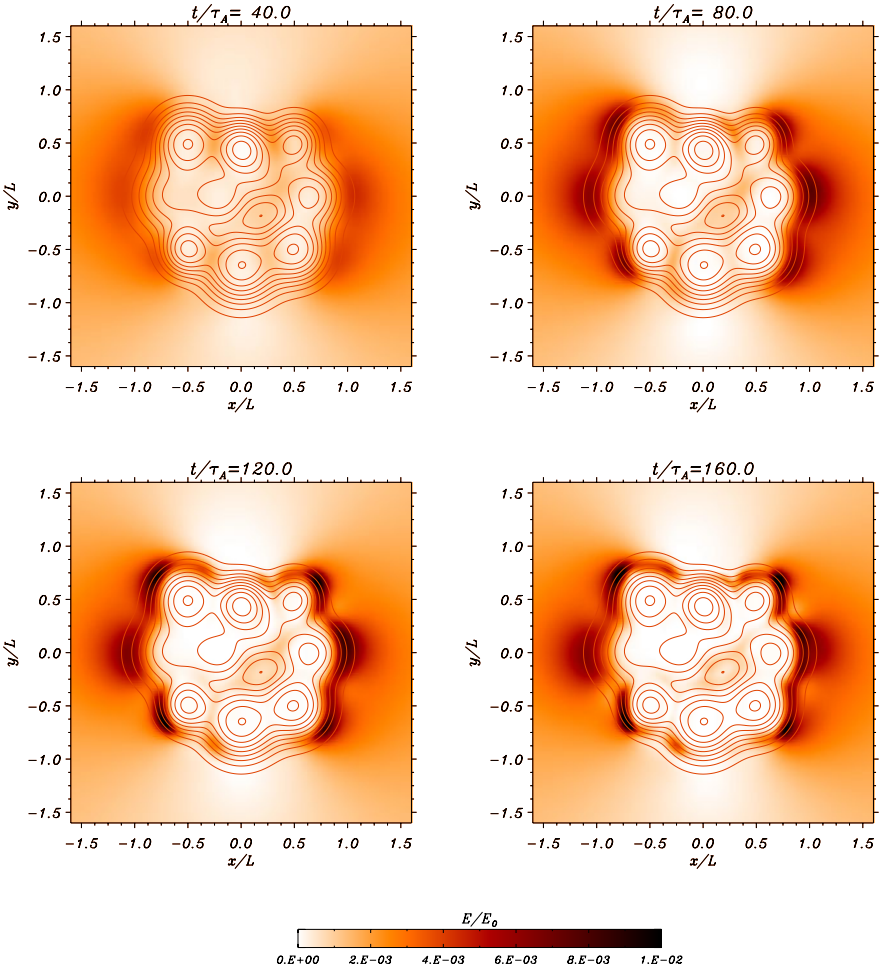

Figure 4. Time evolution of the energy distribution for the same simulation as in Fig. 3. Due to the mode conversion between the global and the localised modes, the energy tends to be concentrated around the resonant layer (external boundary and the internal hole, see also Fig. 1). On the contrary, the energy decreases in most of the internal parts of the loop. The contours of constant Alfvén frequency are also represented.

Once we know the frequency of the global mode (basically the dominant peak on the top right panel of Fig. 2) the location of the resonance involving the quasi-mode can be

https://doi.org/10.1017/S1743921308014762 Published online by Cambridge University Press

determined. In Fig. 1 contours of the Alfvén frequency (ω_A) are represented together with this global frequency (see the contour with the thick line). In this figure we see where the energy conversion takes place, basically at the external edge of the loop but in addition some part of the energy is deposited inside the loop (see the small hole around $x = 0.25L$, $y = -0.25L$), which is precisely where the energy maps show a location of enhanced energy. Thus, for this particular multi-stranded model resonant absorption not only takes place at the external boundaries, some energy is also deposited in the internal part of the loop. This demonstrates that resonant absorption works even in quite irregular geometries like the one studied in this paper and that regular magnetic surfaces (considered in previous works) are not necessary for this mechanism to work efficiently. Further details will be given in a forthcoming paper (Terradas *et al.* 2007).

Acknowledgements

J. Terradas is grateful to the Spanish Ministry of Education and Science for the funding provided under the Juan de la Cierva program. Funding provided under grants AYA2006-07637, of the Spanish Ministry of Education and Science, and PCTIB-2005GC3-03, of the Conselleria d'Economia, Hisenda i Innovació of the Government of the Balearic Islands, is also acknowledged.

References

Andries, J., Goossens, M., Hollweg, J. V., Arregui, I., & Van Doorsselaere, T. 2005, *A&A*, 430, 1109

Arregui, I., Van Doorsselaere, T., Andries, J., Goossens, M., & Kimpe, D. 2005, *A&A*, 441, 361

Arregui, I., Terradas, J., Oliver, R., & Ballester, J. L. 2007, *A&A*, 466, 1145

Aschwanden, M. J. 2005, *ApJ*, 634, L193

Aschwanden, M. J., & Nightingale, R. W. 2005, *ApJ*, 633, 499

Erdélyi, R., & Goossens, M. 1996, *A&A*, 313, 664

Goossens, M., Hollweg, J. V., & Sakurai, T. 1992, *A&A*, 138, 233

Goossens, M., & De Groof, A. 2001, *Phys. Plasmas*, 8, 2371

Goossens, M., Andries, J., & Aschwanden, M. J. 2002, *Solar Phys.*, 394, L39

Hollweg, J. V., & Yang, G. 1988, *JGR*, 93, A6, 5423

Hollweg, J. V., Yang, G., Cadez, V. M., & Gakovic, B. 1990, *ApJ*, 349, 335

Klimchuck, J. A. 2006, *Solar Phys.*, 234, 41

Leveque, R., *Finite Volume Methods for Hyperbolic Problems*, Cambridge University Press, Cambridge, 2002

Mann, I. R., Wright, A. N., & Cally, P. S. 1995, *JGR*, 100, A10, 19 441

Martens, P. C. H., Cirtain, J. W., & Schmelz, J. T. 2002, *ApJ*, 577, L115

Ruderman, M. S. 2003, *A&A*, 409, 287

Ruderman, M. S., & Roberts, B. 2002, *ApJ* , 577, 129

Ruderman, M. S., & Erdélyi, R., in (sci-eds) R. Erdélyi, J. L. Ballester, B. Fleck, *Waves, Oscillations and Small-Scale Transient Events in the Solar Atmosphere: A Joint View from SOHO and TRACE*, ESA-SP 547, 507, 2004

Schmelz, J. T., Nasraoui, K., Richardson, V. L. *et al.* 2005, *ApJ*, 627, L81

Terradas, J., Oliver, R., & Ballester J. L. 2006a, *ApJ*, 642, 533

Terradas, J., Oliver, R., & Ballester J. L. 2006b, *ApJ*, 650, L91

Terradas, J., Arregui, I., Oliver, R., & Ballester J. L. 2007, in preparation

Tirry, W. J., Berghmans, D., & Goossens, M. 1997, *A&A*, 322, 329

Van Doorsselaere, Andries, J., Poedts, S., & Goossens, M. 2004, *ApJ*, 606, 1223